



## Research article

# Combined strategy for tuning sensor-less brushless DC motor using SEPIC converter to reduce torque ripple

A. Prakash<sup>a,\*</sup>, C. Naveen<sup>b</sup><sup>a</sup> Department of Electrical and Electronics Engineering, QJS College of Engineering & Technology, Ongole, Andhra Pradesh, India<sup>b</sup> Department of Electrical and Electronics Engineering, SRM Institute of Science and Technology, Chengalpattu, India

## ARTICLE INFO

## Article history:

Received 12 April 2022

Received in revised form 29 June 2022

Accepted 29 June 2022

Available online 2 July 2022

## Keywords:

Speed control

Torque ripple minimization

Golden Eagle Optimization

Radial Basis Function Neural Network

Modified bridgeless SEPIC converter

## ABSTRACT

The brushless DC motor (BLDCM) is widely used in computer numerical control (CNC) machines, aerospace applications and auto industry applications in the field of robotics. But it is still affected by the transmission torque ripple, which mostly depends on the speed and the transient line current at the transmission interval. This manuscript proposes a combined approach for tuning sensor-less brushless DC (BLDC) motors using a single-ended primary-inductor converter (SEPIC). The proposed technique is a combination of Golden Eagle Optimization (GEO) and Radial Basis Function Neural Network (RBFNN), hence it is called GEO-RPFNN. The control of speed and torque is to reduce the torque ripple in the motor. Here, the modified bridgeless single-ended primary-inductor converter is proposed to improve speed and torque control. The proposed method is used to adjust the parameters of proportional integral derivative (PID) controller and to improve the performance of PID controller. Therefore, the GEO-RBFNN technique is proposed to recover the control loop function. The proposed algorithm is explored to control the speed and torque error as BLDC motor. Nevertheless, the output of the proposed approach is subject to the input of speed and torque controllers. The proposed method is executed in MATLAB Simulink site. The performance of the proposed system is compared with existing FA and PSO methods. As per the state of comparison outcomes, the GEO-RBFNN gives better result than the existing techniques which has higher ability to conquer the related issues. The THD in stator current, power factor and torque ripple gives the value using proposed method is 1.26%, 0.9951 and 7.4.

© 2022 ISA. Published by Elsevier Ltd. All rights reserved.

## 1. Introduction

Recently, the usage of BLDC motor is increased in various applications, such as aerospace application, automotive industry, robotics, medical instrument, electric vehicle (EV) utilization. Owing to the simple speed control, the BLDC motor is used in many applications [1]. The design model of brushless DC motor is similar to permanent magnet synchronous motor (PMSM). The coil is located in the stator, whereas permanent magnet is located in the rotor. Based on the location of rotor, the working of BLDC motor takes place [2]. The location of rotor is identified using Hall Effect sensors. The control of BLDC motor is important to gather better reaction of torque with speed and minimize the ripple [3–5]. The stator current loss creates ripples, which trigger to generate variations and disturbances on the motor. So, there is a chance to decrease the usage of BLDC motor in few applications [6].

The minimization of ripple is the most important work in BLDC motor. Due to lesser cost requirements, less interruptions, better lifetime, greater efficiency and power density, the BLDC motor is used in many applications [7–10]. The rotor data is obtained through the hall sensors. These sensors are affected by electro-magnetic interference (EMI) error and implementation error. In addition, the high heat issues may affect the sensor operation. To overcome these drawbacks, many sensors-less equipment's are introduced. In recent days, the sensor-less BLDC motor is used in multiple works to control the speed and minimize the ripples [11]. The main disadvantage of sensor-less BLDC is the identification of rotor position that is possible only during minimum speed operation. Because of the magnetic displacement along winding operations, BLDC basically have a non-sinusoidal back electromagnetic force (EMF), which needs accurate control to increase the stable torque. Mainly, the stator current with back EMF creates ripples on the rotor place. The major problem of torque ripple is overload, acoustic noise generation, and higher variations in the systems. The torque ripple is one of the critical problem in BLDC created by unequal commutating phase current shift error and phase current rate [12–15].

\* Corresponding author.

E-mail address: [prksh830@gmail.com](mailto:prksh830@gmail.com) (A. Prakash).

Generally, BLDC motor is a synchronous motor that obtains the DC power through an inverter or switch and distribute the AC power to enhance every phase of the stator winding via the control loop [16]. The PID controllers are basically employed to adjust the speed, torque and lessen the ripples [17–20].

### Objectives and contribution

- (a) A combined GEO–RBFNN converter is proposed to tune sensor-less Brushless DC motor using SEPIC. The proposed system is the joint implementation of GEO and RBFNN. The GEO–RBFNN is activated in MATLAB/Simulink working platform; its effectiveness is compared to the existing systems.
- (b) The innovation of proposed system is search space that is increased through the operation of GEO and the optimal solution established this golden eagle search space.
- (c) The proposed study has two major functions to deal the optimization issue. The control of speed and torque and torque ripple minimization are accomplished by using the GEO–RBFNN algorithm.
- (d) The effectiveness based on effect of rotor speed, torque variation, stator current, stator EMF are analyzed without controller and various solution techniques. Furthermore, speed and torque control of proposed and existing systems are also investigated.

Remaining manuscripts is arranged as: Section 2 delineates the recent studies, Section 3 describes the configuration of bidirectional power sharing control, Section 4 explains the proposed strategy of GEO–RBFNN, Section 5 demonstrates outcomes and discussion, Section 6 concludes the manuscript.

## 2. Recent research works: A brief review

Various studies previously presented on literatures were related to bidirectional power sharing control. Here a part of them are revised:

Khazaei et al. [21] have presented the direct torque control of BLDC motor drive using maximum torque per ampere (MTPA) strategy. The MTPA control technique was presented to control the speed with torque ripple. Also, Lagrange's theorem was presented to identify the MTPA parameters that triggered the parameters to become 0 and give promising solutions to MTPA method. Ganesan et al. [22] have suggested the ANFIS based multi-sector space vector PWM system (MS-SVPWM) of sensor-less BLDC motor drive. The MS-SVPWM technique was suggested for controlling the operation of BLDC motor. The motor contains uncontrolled rectifier part to give direct current source to inverter part. The speed control of BLDC motor was accomplished using MS-SVPWM with ANFIS controller. The major role of ANFIS controller was choose the match-able section and identify the unrelated pulses through the comparison operation. Senthilnathan and Palanivel [23] have demonstrated a novel strategy of commutation torque ripple reduction of FPGA fed BLDC motor. The OCDHC technique was introduced to lessen the processing time and torque ripple. The coding was written in VHDL platform and the result was given to FPGA. FPGA obtain hall sensor output and current BLDC motor using lower torque ripple.

Patel and Chandwani [24] have suggested a modified sinusoidal pulse width modulation (PWM) system for torque ripple attenuation on BLDC. The MSPWM method was employed for controlling speed and lessens ripples of BLDC motor. The speed control was attained using PI controller. The hall sensor was used to identify the correct location and speed of the rotor. Zhang and Li [25] have presented a rapid commutation error compensation system of sensor-less control for MSCMG BLDC Motor using

Non-ideal Back-EMF. The quick commutation error compensation process was presented to increase the accuracy. Initially, the buck converter and commutation points calculating circuit were implemented. The ESO was used to analyze the DC voltage. Kommula and Kota [26] have suggested a direct instantaneous torque control of BLDC motor with firefly Algorithm (FA) fed Fractional order PID controller (FOPID). The FOPID controller was used to tune the BLDC parameters. The reduction of torque ripple with speed control was achieved by FA algorithm. The computation of torque ripple was done with direct manner also the output was provided to FOPID controller for tuning purpose. The FA approach was used to tune the FOPID criterions. de Castro et al. [27] have presented the enhanced finite control-set model based on direct power control of BLDC Motor. The FOC or DTC techniques were presented to overcome the BLDC speed control and torque reduction problems. Large bandwidth controllers were needed to analyze the correct input voltage during ripple reduction operation. To overcome these drawbacks, FCS-MPC method was presented to achieve quick torque reaction and provides better performance.

Dasari et al. [28] have presented the Smart controller for BLDC Motor Drive System Speed Regulation by Multi-Purpose Feature was suggested. The presented method accurately improves the levels of voltage source inverter direct current provides correct operations of motor. The optimal gain parameters needs FOPID controller to lessen the torque ripples and control the speed of BLDC motor. Firstly, the nature-inspired optimization method of Elephant herding optimization was examined to find the error function. Also, the effective Adaptive neuro-fuzzy inference system controller lessens the systematic method to track the error functions for providing finest optimum gain values. Using the control method, the Harmonics and torque ripples were reduced. The output of speed and torque was analyzed based on control scheme. Santra et al. [29] have presented a novel switching method to lessen the losses in trapezoidal BLDC motor drive. Based on analysis, a pulse bandwidth modulation (PWM) system with selective harmonics elimination (SHE) was provided for motor phase current and dynamic loss reduction of the brushless DC motor drive system.

### 2.1. Background of the research work

The speed control and torque ripple minimization of sensor-less brushless DC motor are the significant strategies for protecting system as numerous involving factors. Based on the bibliography observation of various speed and torque ripple control methods, like maximum torque per ampere (MTPA), multi-sector space vector PWM (MS-SVPWM) scheme, outgoing-phase current discharge hysteresis control (OCDHC), FOPID controller, firefly algorithm (FA) etc. The main aim of MTPA methods identifies the current operating point and also it is used to control the maximum torque with constant stator current amplitude. But the optimal position encoder is required for providing optimal result. The MS-SVPWM technique is used to minimize the dc voltage ripple and total harmonic distortions, but it uses small DC bus to transmit. Also, the Hysteresis Current control is used to manage sending and receiving phase current with equal speed at whole commutation time. Furthermore, it is used to minimize the commutation torque ripple and transmit accurate commutation, but the frequency variations are occurred during the process. FOPID controller is used to tune the control parameters of BLDC motor minimize the error generation during the process. The implementation process of FOPID is based on the frequency domain analysis. In fire-fly algorithm, the light intensity and the brightness of fireflies are calculated. If the light intensity is increased, then the brightness of fireflies is also increased and the performance of objective function is increased. When the

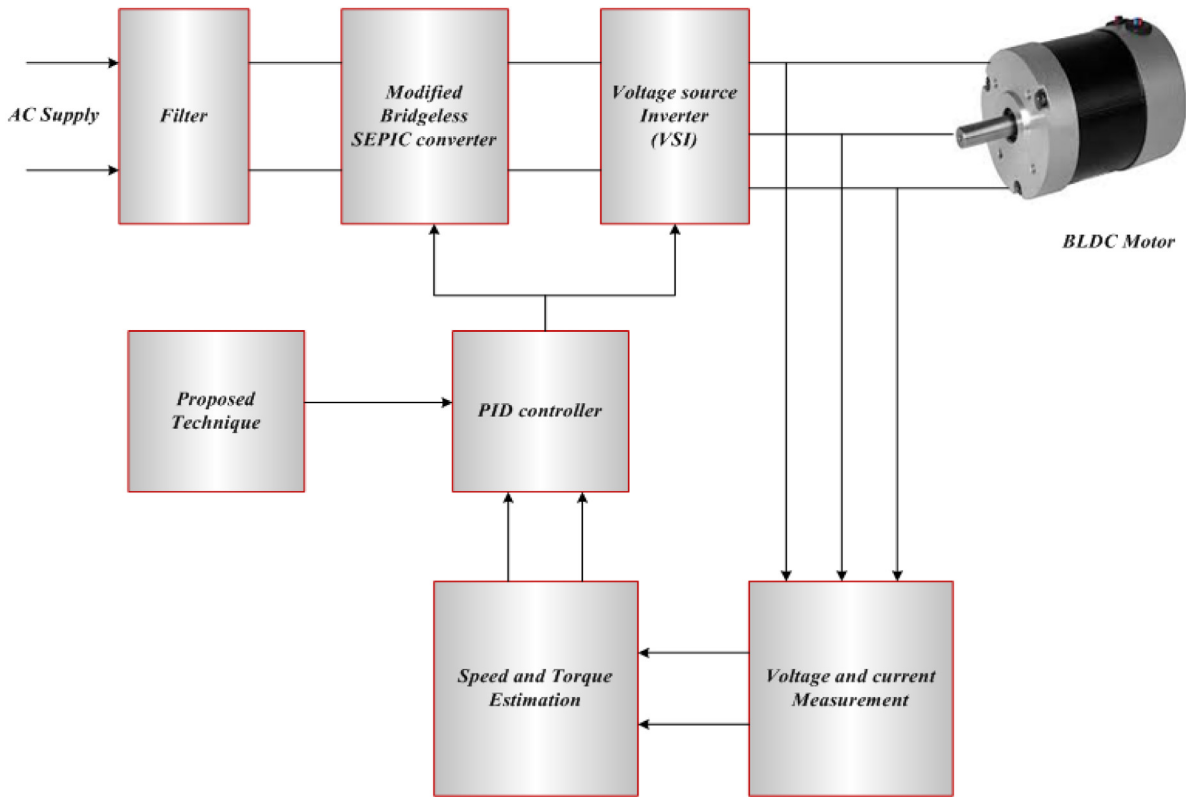


Fig. 1. The proposed control structure of sensor-less brushless DC motor.

performance is decreased its intensity is decreased. Therefore, the tuning of sensor-less BLDC motor using GEO–RBFNN is required for a promising solution to overcome these drawbacks. The aim is to improve the disadvantages observed in the literature works by suggesting a novel instantaneous torque control. The torque is instantly controlled with torque controller by integral variable structure control (IVSC) and space vector pulse width modulation (SVPWM). In literature works, the utilized technique is complex and also produces high torque ripple. All the above studies depend on current setup and moderately complicated. All of the beyond systems suffer as slow voltage adjustment may only accomplish acceptable suppression of torque pulsations under minimum or maximum speed areas. The above methods are used to lessen the ripple of switching torque and shorten the switching time. Though, DC/DC converters deliver full power on switching period, increasing the rating of power components and reducing the reliability of electronic device. Few works based on methodologies were exhibited in the literatures solves this problem; these difficulty and problems motivated this investigate work.

### 3. Sensor-less BLDC motor tuning configuration

In this manuscript, to control the torque and speed to lessen the torque ripple in sensor-less BLDC motor, the GEO–RBFNN method based PID controller is proposed. The proposed control structure of sensor-less BLDC motor portrayed in Fig. 1. Here, the Alternating current is considered as input of system. Initially, an Alternating Current input signal is given to the filter. The filter has the ability to reduce the unwanted signals and the filter output is given to the input of SEPIC converter. The SEPIC converter increases the speed and torque performance also gives the output to VSI.

The output of VSI is provided with BLDC motor. Here, the PID controller acts as the proposed controller to tune control parameters. The proposed PID controller produce the PWM signals for optimal tuning of control parameter, which provides PWM signal to modified Bridgeless SEPIC converter for optimal speed control and torque ripple reduction of sensor-less BLDC motor.

#### 3.1. Mathematic modeling of BLDC motor

The mathematic model is needed for analyzing and controlling the performance of BLDC motor. It is considered that every stator phase winding has a resistance corresponding to one phase and that the self-inductances and mutual inductance are constant and the iron loss is very small. Due to incomplete motor flux and the optimal power semiconductor equipment, the following expressions demonstrate the computer features, which shows in [30],

$$\frac{\partial I_A}{\partial T} = \frac{1}{l - m} [-rI_A + v_A - E_A] \tag{1}$$

$$\frac{\partial I_B}{\partial T} = \frac{1}{l - m} [-rI_B + v_B - E_B] \tag{2}$$

$$\frac{\partial I_C}{\partial T} = \frac{1}{l - m} [-rI_C + v_C - E_C] \tag{3}$$

$$\frac{\partial \omega_R}{\partial T} = -\frac{1}{j} [b\omega_R + t_l] \tag{4}$$

$$\frac{\partial \varphi_R}{\partial T} = \frac{p}{2} \omega_R \tag{5}$$

where  $E_A, E_B, E_C$  is represented as back EMF,  $m$  denotes the mutual inductance,  $I_A, I_B,$  and  $I_C$  is phase currents,  $l$  represents self-inductance,  $p$  implies number of poles,  $b$  is friction constant,  $\omega$  implies angular velocity,  $\varphi$  denotes rotor position,  $j$  implies rotor inertia, and  $t_l$  implies load torque.

### 3.2. Sensor-less BLDC motor

The identification of rotor position is important for BLDC motor to deliver optimal commutation signals to all part of the circuit. Due to the difficult setup with higher cost of rotor position sensors, the performance of BLDC motor is reduced. The sensor-less BLDC motor is introduced to overcome these drawbacks. The sensor-less BLDC motor is used to minimize the hardware issues and gives the promising solution to reliable power transmission within the systems. The sensor-less BLDC motor takes energy from trapezoidal back electromagnetic force, which is generated from the mobility of permanent magnet rotor. That minimizes the difficulties of variations from each sensor. The computation of speed, torque, flux of sensor-less BLDC motor can be done with the help of terminal voltages and input current.

### 3.3. PID controller

To control the processing parameters, like speed and torque of sensor-less BLDC motor, proportional integral derivative controller is used. The controlling process is done with the help of feedback devices. The parameter control provides a way to achieve the significant output. The main function of proportional integral derivative controller triggers the feedback device to achieve fixed result. The three parameters of proportional integral derivative controller is proportional ( $K_p$ ), integral ( $K_i$ ), and derivative ( $K_d$ ) gains. The transfer function of PID controller is denoted as,

$$G(S) = \frac{U(S)}{E(S)} = K_p \left[ 1 + \frac{1}{T_i S} + T_d S \right] \quad (6)$$

here  $K_i = \frac{K_p}{T_i}$  and  $K_d = K_p T_d$

Basically, the PID controller is used to enhance the behavior of speed control. The PID controller's performance can be improved by proper tuning of its parameters, such as  $K_p$ ,  $K_i$ ,  $K_d$ . Here, the optimal tuning of proportional integral derivative parameters, the GEO-RBFNN technique is used. In this manuscript, the proposed GEO-RBFNN based PID controller is used to control its speed and torque, also it lessens the torque ripple of BLDC motor.

### 3.4. Speed control strategy

At the processing of brushless dc motor, the speed is computed based on sensor-less method. The speed error is minimized with the help of GEO-RBFNN technique. Here, SEPIC converter is introduced to convert DC voltage into DC voltage. The switch is either in ON or OFF conditions. The switching actions are calculated based on the rotor position to control the direction of rotation, speed and torque of motor. In sensor-less method, the actual rotor speed is computed in terms of voltage and the current values calculated by motor. The error calculation provides the original speed such that the speed computed by the sensor-less method and the reference speed is fixed manually. By comparing the two speeds, the error detection provides the speed error which can be expressed as,

$$\omega_{ERROR} = (\omega^* - \omega) \quad (7)$$

where  $\omega$  is referred as the actual speed that is calculated from motor parameters, like terminal voltage and current in fluctuation load setting, the reference speed implies  $\omega^*$  and  $\omega_{ERROR}$  represented as brushless dc motor error speed value.

### 3.5. Design of torque controller system

The speed and torque control is the required task of BLDC motor that increases the performance of brushless motor; also it triggers to increase the usage of brushless dc motor in various applications. If the control operation is failed, the torque ripples are generated to diminish the performance of BLDC motor. So the minimization of torque ripple is the required task of BLDC motor. The Direct Torque Control method (DTC) is employed due to its higher accuracy and lower computational issues. The torque ripple of BLDC motor can be expressed as [31].

$$T_{E(RIPPLE)} = \frac{1}{2} \int_{NT_E}^{(N+1)T_E} (T_E - T_E^*)^2 \partial T \quad (8)$$

$$T_{ERROR} = (T^* - T) \quad (9)$$

where  $T_E$  represents the EM torque,  $T_{E(RIPPLE)}$  is the EM torque ripple,  $T_{ERROR}$  is the torque error,  $T^*$  is represents the reference value of torque, and  $T$  represents real value of torque.

### 3.6. Modified bridgeless SEPIC converter

In this manuscript, a modified bridgeless SEPIC converter with inductor is implemented to control the speed with torque of BLDC motor utilizing pulse width modulation. One core is used to close two inductors.

Fig. 2 depicts circuit diagram of SEPIC through BLDC motor. So, the size and weight is also decreased that helps to minimize the self-induction value. Furthermore, the torque ripple is also minimized, so that the performance of BLDC motor is increased.

#### 3.6.1. Operation of bridgeless SEPIC converter

Inside the bridgeless SEPIC with joined inductors, PWM controller is working to achieve DC bus voltage ( $v_{DC}$ ) in excess of a wide range of speed through modified duty cycle of power devices. The circuit configuration of BLDC motor at the intervals of positive half cycle (Switch On, Diode Off) is depicted in Fig. 3. The Circuit configuration of BLDC motor at intervals of positive half cycle (Switch Off, Diode ON) is shown in Fig. 4. Circuit configuration of BLDC motor at intervals of positive half cycle (Switch Off, Diode Off) is shown in Fig. 5. In Figs. 3–5, the implementation of bridgeless SEPIC converter can be viewed as dual SEPIC converter, one of which works through the positive half-cycle for voltage supplying and converter works at negative half-cycle for voltage supplying. The SEPIC converter with the components  $L_{11}$ ,  $L_{01}$ ,  $C_1$ ,  $C_D$ ,  $D_1$ , and  $SW_1$  works at positive half cycle supply. Diode finishes the way of positive half cycle for supplying [32]. At another cycle, the components  $L_{12}$ ,  $L_{02}$ ,  $C_2$ ,  $C_D$ ,  $D_2$  and  $SW_2$  are working with rectifier diode. The magnetic connection among dual inductors is shown in dotted line. When the inductors combined, it has mutual inductance, also when the inductors are connected; the mutual induction is created among the coils. The SEPIC DCM function has three intervals in every transition cycle.

#### Interval 1

At interval 1, the  $SW_1$  is ON and  $D_1$  is OFF are shown in Fig. 3 and the inductors ( $L_{11}$ ) and  $L_{01}$  begins to charge. The middle capacitor ( $C_1$ ) release their charge through the inductor  $L_{01}$  at destination part, so the voltage across it begins to reduce.

#### Interval 2

At interval 2, the  $SW_1$  is OFF, and  $D_1$  is ON are shown in Fig. 4 and the inductors ( $L_{11}$ ) and  $L_{01}$  at load side begins to discharge through  $D_1$ . The capacitors  $C_1$  and  $C_D$  is also charging during this period.

#### Interval 3

At interval 3,  $SW_1$  and  $D_1$  are OFF condition as shown in Fig. 5. The inductors ( $L_{11}$ ) and  $L_{01}$  are totally release their charges. A non-zero residual current can run via the inductors and middle capacitor.

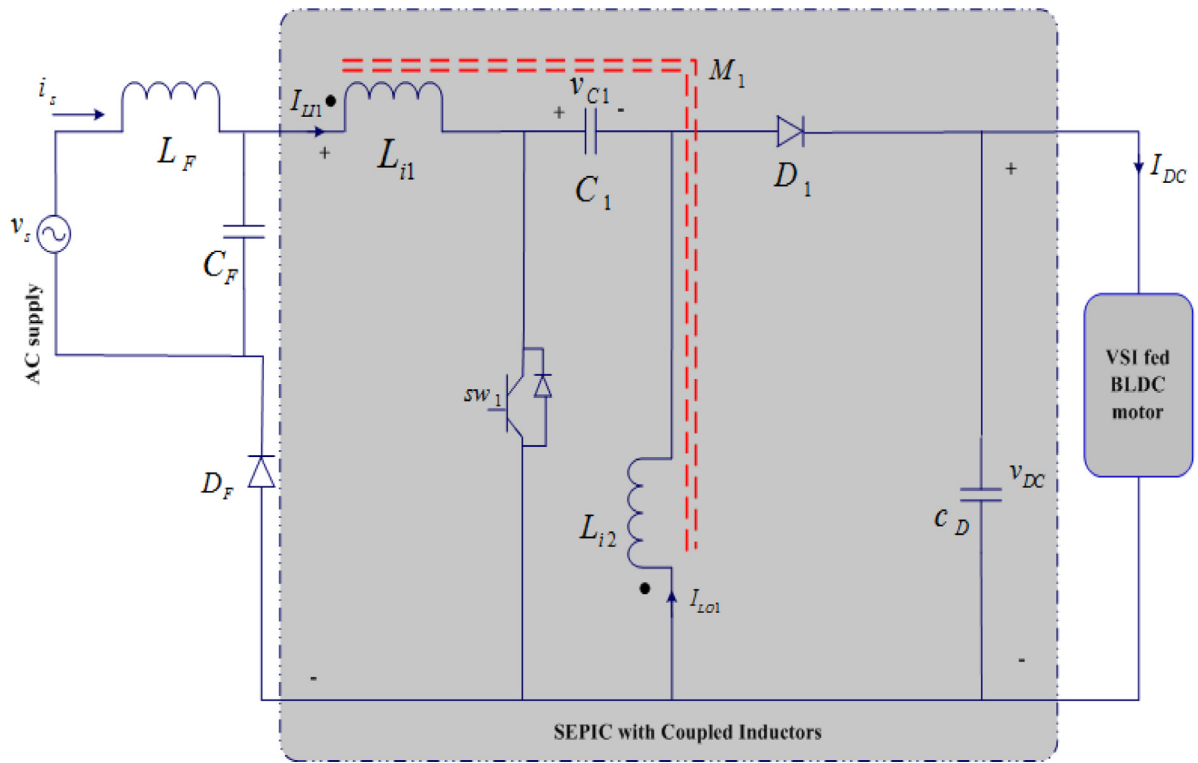


Fig. 2. Positive half cycle process of bridgeless SEPIC.

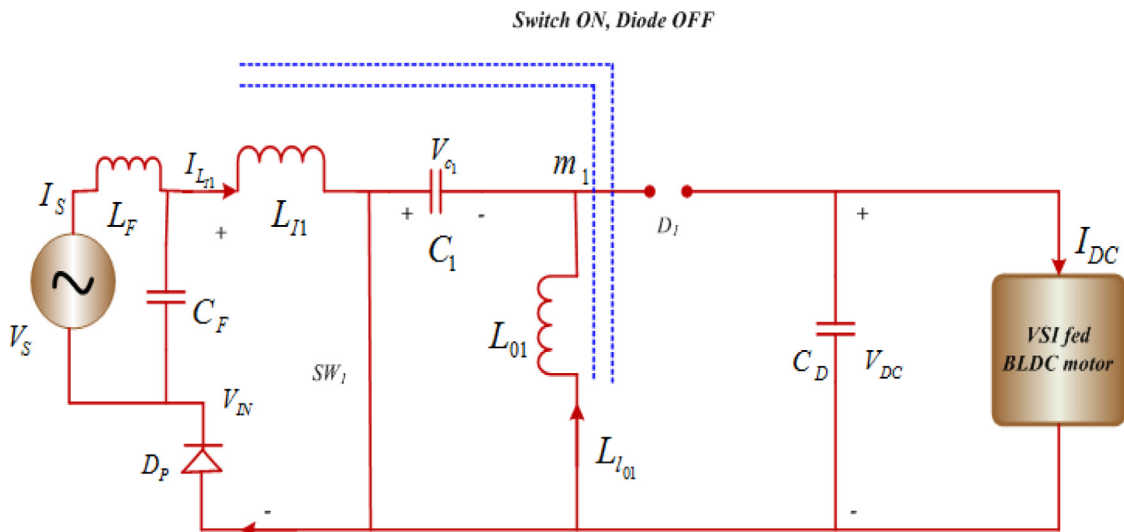


Fig. 3. BLDC motor at intervals of positive half cycle (Switch On, Diode Off).

3.6.2. Impact of coupled inductors in single-ended primary-inductor converter topology

The working process of positive half cycle is assumed to analyze the result of coupled inductors on SEPIC converter. There are two inductors are involved in the SEPIC converter they are, (i) inductor along self-inductance at input ( $L_{i1}$ ), (ii) inductor along self-inductance at output ( $L_{o1}$ ). The coupling coefficient and mutual inductance is expressed as  $k_{c1}$  and  $M_1$ .

$$k_{c1} = \frac{M_1}{\sqrt{L_{i1}L_{o1}}} \tag{10}$$

Then, the ratio of the turns of two windings  $n_1$  is given by,

$$n_1 = \frac{v_{L_{o1}}}{v_{L_{i1}}} = \frac{N_{o1}}{N_{i1}} = \sqrt{\frac{L_{o1}}{L_{i1}}} \tag{11}$$

here voltage across the inductor ( $L_{o1}$ ) and ( $L_{i1}$ ) is expressed as  $v_{L_{o1}}$  and  $v_{L_{i1}}$ , number of turns of coupled inductors ( $L_{o1}$ ) and ( $L_{i1}$ ) is expressed as ( $N_{o1}$ ) and ( $N_{i1}$ ). Voltage across coupled inductor windings contain self-inductances ( $L_{o1}$ ) and ( $L_{i1}$ ) are provided in the Eqs. (12) and (13).

$$v_{L_{i1}} = L_{i1} \frac{di_{i1}}{dt} + M_1 \frac{di_{o1}}{dt} \tag{12}$$

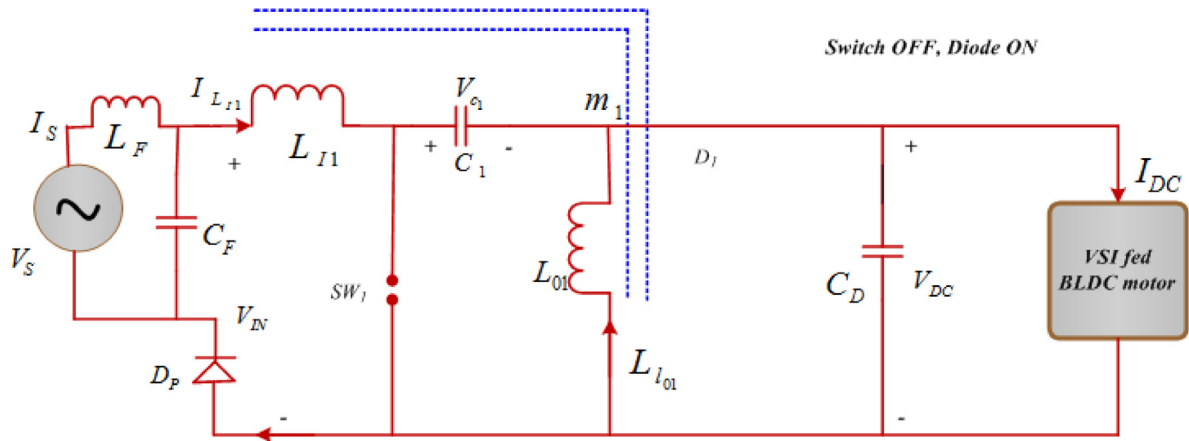


Fig. 4. BLDC motor at intervals of positive half cycle (Switch Off, Diode ON).

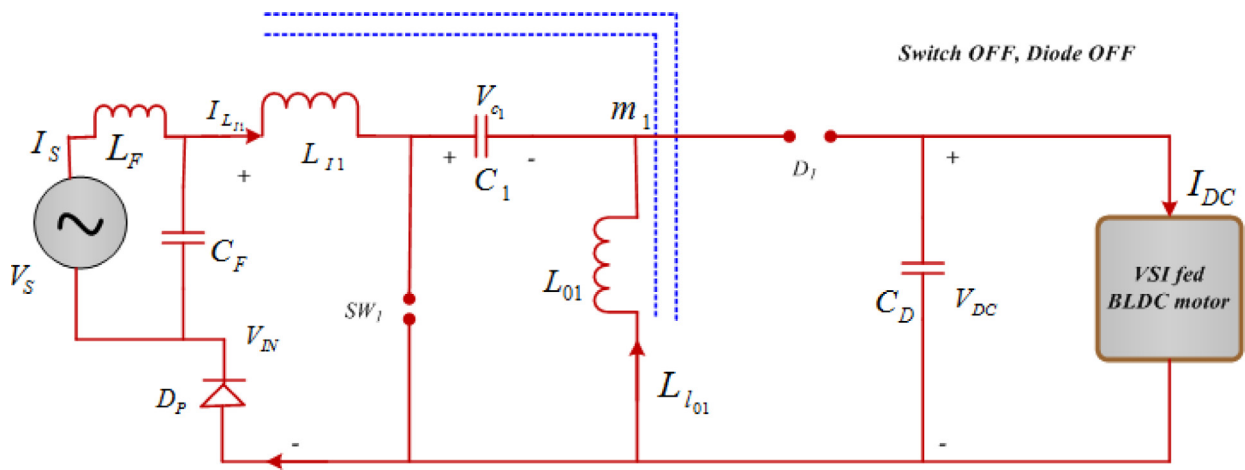


Fig. 5. BLDC motor at intervals of positive half cycle (Switch Off, Diode Off).

$$v_{L_{O1}} = M_1 \frac{di_i}{dt} + L_{O1} \frac{di_{O1}}{dt} \tag{13}$$

In every interval of the switching cycle, the voltage across the two inductors is same and it is given in the following equation,

$$v_{L_{I1}} = v_{L_{O1}} \tag{14}$$

If it satisfies the relationship given by the Eq. (15), then the coupled inductors can attain zero ripple.

$$\frac{v_{L_{I1}}}{v_{L_{O1}}} = 1 = \frac{M_1}{L_{O1}} = k_{c1} \sqrt{\frac{L_{I1}}{L_{O1}}} \tag{15}$$

The following equations are formed by substituting the Eq. (14) into Eqs. (12) and (13).

$$\frac{di_{L_{I1}}}{dt} = \frac{v_{L_{O1}}L_{O1} - v_{L_{I1}}M_1}{L_{I1} * L_{O1} - M_1^2} = \frac{v_{L_{O1}} - \frac{k_{c1} * v_{L_{O1}}}{n_1}}{L_{I1}(1 - k_{c1}^2)} \tag{16}$$

$$\frac{di_{L_{O1}}}{dt} = \frac{v_{L_{I1}}L_{I1} - v_{L_{O1}}M_1}{L_{I1} * L_{O1} - M_1^2} = \frac{v_{L_{O1}} - k_{c1} * v_{L_{I1}} * n_1}{L_{O1}(1 - k_{c1}^2)} \tag{17}$$

The equivalent inductance model can be derived in the following,

$$L_{I1eq} = L_{I1} \frac{1 - k_{c1}^2}{1 - \frac{k_{c1}}{n_1}} \tag{18}$$

$$L_{O1eq} = L_{O1} \frac{1 - k_{c1}^2}{1 - n_1 k_{c1}} \tag{19}$$

here equivalent inductance values produced based on coupling can be written as  $L_{I1eq}$  and  $L_{O1eq}$ . Likewise, the corresponding inductance values created the result of coupling for converter processing at negative half cycle is referred from Ref. [33].

### 3.6.3. Bridgeless SEPIC topology design using coupled inductors of BLDC drive

The bridgeless single-ended primary-inductor converter is designed using the coupled inductor to broad range of output voltage control. The converter process is guaranteed at DCM to the total dc voltage range. So, it attains auto-shape of distributed current. The function of duty ratio is the output DC voltage and it is given by,

$$V_{dc} = \frac{D}{(1 - D)} V_{in} \tag{20}$$

here input voltage mean value with SEPIC converter as  $V_{in}$ . For ripple current of  $\Delta I_{Lin}$ , the input side inductors are designed by,

$$L_{I1eq} = L_{I2eq} = \frac{V_{in} * D}{\Delta I_{Lin} * I_{in} * f_s} \tag{21}$$

here  $I_{in} = \frac{P_{in}}{V_{in}}$  and  $P_i = \frac{P_{max}}{V_{dc,max}}$  is the input power for any values of DC voltage. The inductor in the output side is given in the following equation,

$$L_{O1eq} = L_{O2eq} = \frac{V_s^2 * V_{dc} * D}{P_i * 2 * I_{in} * f_s} \tag{22}$$

where RMS value of supply voltage is given as  $V_s$ . By then the intermediate capacitance with ripple voltage, DC link capacitor, design of filter capacitance performed their maximal value and the design of filter inductance is referred from the Ref. [33].

**4. Proposed method of golden eagle optimization (GEO) algorithm and radial basis function neural network (RBFNN)**

For controlling speed and torque of sensor-less BLDC motor, GEO–RBFNN is implemented. The integration of GEO and RBFNN optimally control speed and torque of sensor-less brushless motor. Here, GEO acts as an important role to tune the control parameters. The output of GEO is given to the RBFNN for accurate result. The RBFNN makes testing and training function. Then, finally selects the optimal value for increasing the performance of sensor-less BLDC motor.

*4.1. Processing steps of golden eagle optimization algorithm*

The common characteristics of GE is cruising and hunting. All golden eagles are flying at high altitude within their circle path and search the prey. When it finds the prey, it notes the location of the prey. Then, it slowly reduced their altitude and moves towards the prey. At the same time, the golden eagle searches the surrounding places for better prey [34]. If it does not find any other better prey, it continues to moves towards the targeted prey and attack that prey. If it finds the better one, then moves towards the area of better prey and rejects the previous prey from its target list. The step wise process of GEO is as follows,

**Step 1:** Initialization

The initial population of distributed Golden eagle is generated uniformly. The outdoor speed control loop has proportional integral controller, which is utilized to create indoor voltage control loop reference dc voltage. It makes easy to control the bridgeless SEPIC converter output voltage to accomplish dc link voltage control.

**Step 2:** Random Generation

The PI controller gain parameters are randomly generated. Here, the current and voltages are randomly created with below matrix Z:

$$Z = \begin{bmatrix} K_p^{11}(t)K_i^{11}(t) & K_p^{12}(t)K_i^{12}(t) & \dots & K_p^{1m}(t)K_i^{1m}(t) \\ K_p^{21}(t)K_i^{21}(t) & K_p^{22}(t)K_i^{22}(t) & \dots & K_p^{2m}(t)K_i^{2m}(t) \\ \vdots & \vdots & & \\ K_p^{n1}(t)K_i^{n1}(t) & K_p^{n2}(t)K_i^{n2}(t) & \dots & K_p^{nm}(t)K_i^{nm}(t) \end{bmatrix} \quad (23)$$

where  $K_p(t)K_i(t)$  denotes PI controller gain parameters.

**Step 3:** Fitness Function

From the initialized values, the fitness function equation is expressed as,

$$F_{Best} = MIN(Error) \quad (24)$$

where

$$Error = \begin{bmatrix} R_1^{MAX} - R_1^{ACT} \\ R_2^{MAX} - R_2^{ACT} \\ R_L^{MAX} - R_L^{ACT} \\ R_{IC}^{MAX} - R_{IC}^{ACT} \end{bmatrix}$$

**Step 4:** The spiral motion of golden eagles (GEs)

Golden eagle optimization is depends on GEs spiral movement. All GEs learns better place from the place they visited so

far. The eagle attacks the prey and searches better prey in the surroundings simultaneously.

**Step 5:** Prey Selection

At each repetition, every golden eagle selects the prey to carry out cruise and attack operations. Every golden eagle can memorize better solution so that they are established so far. Every search agent chooses a goal prey as whole herd memory. The attack including cruise vectors of every GEs are scaled with chosen prey.

**Step 6:** Attack (Exploitation)

This is modeled via the vector begins as present location of golden eagle and ends at position of prey under eagle memory.

**Step 7:** Cruise (Exploration)

Depending on the attack vector, the cruise vector is determined. The cruise vector is defined as tangent circle as well as it is perpendicular to the vector attack.

**Step 8:** Move to new position

In the fitness of novel GEs position, is better than location at their memory and this eagle’s memory is enhanced by the new position. At the novel repetition, every GE randomly selects a GE as population to circle their better-visited position.

**Step 9:** Transitions from exploration to exploitation

The GEs display greater propensity to cross in beginning stages of hunting flight, also prove better propensity to attack on later stages associated with more exploration on primary repetitions and at proposal optimizer, extra exploitation is present in the final iterations.

**Step10:** Termination

The process continues as step 3 while the torque ripple goes beyond threshold level if not process is completed. Finally, the system has an ability to choose the best control signal of sensor-less BLDC motor with lower error along with system parameters, once the above steps of the algorithm are finished.

*4.2. Processing steps of RBFNN*

The RBFNN is used to control the speed and torque of sensor-less BLDC motor. The RBFNN is the hidden layer of neural networks. Here, the output of GEO is given to the input of RBFNN for the optimal result. The RBFNN performs the testing and training operation on the control signals and finally selects the optimal value to the function [35].

**Step 1:** The number of input nodes are similar to dimension  $X$  of input vector  $A$  specifies initial layer.

**Step 2:** Hidden layer is second layer that directly linked to input nodes.

**Step 3:**  $E(\|A - A_1\|)$  is the output of  $I$ th hidden layer nodes. here,  $A_1 = [a_{11}, a_{12}, \dots, a_{1X}]$  is the center of basic operation.

**Step 4:** The output of the RBFNN is expressed as,

$$R(a_p - C_I) = EXP\left(-\frac{1}{2\xi^2} \|a_p - C_I\|^2\right) \quad (25)$$

where  $a_p$  implies  $P$ th input sample,  $\xi$  implies Gaussian activation function.

$$V_J = \sum_{I=1}^H M_{IJ} EXP\left(-\frac{1}{2\xi^2} \|a_p - C_I\|^2\right) \quad J = 1, 2, \dots, N \quad (26)$$

here  $H$  is the count of nodes in hidden layer. Fig. 6 shows flowchart of . GEO–RBFNN.

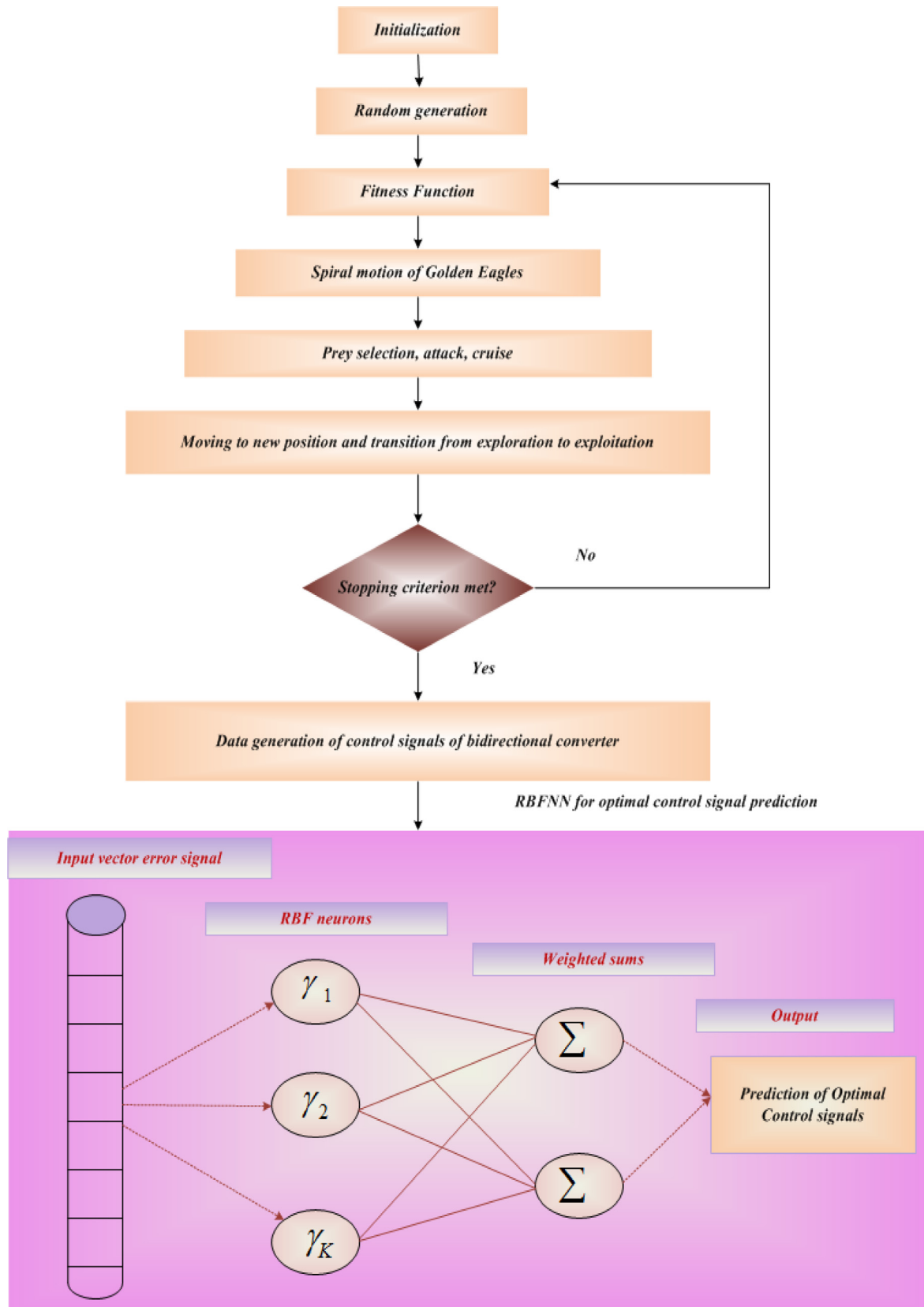


Fig. 6. Flowchart of GEO-RBFNN algorithm.

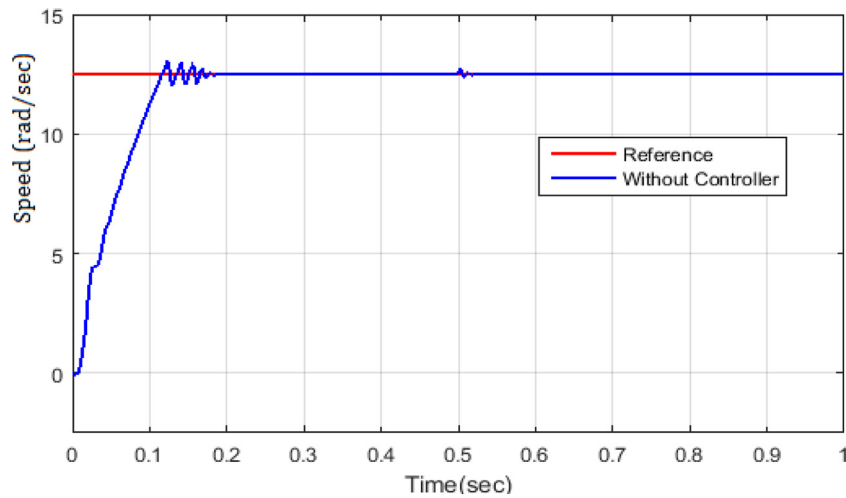


Fig. 7. Impact of rotor speed difference without controller.

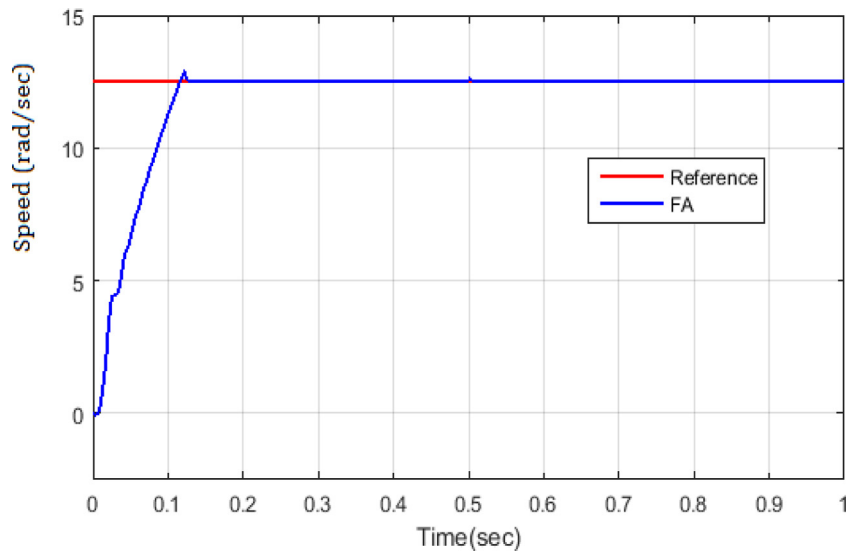


Fig. 8. Result of rotor speed difference of existing FA method.

5. Result with discussion

The proposed GEO–RBFNN is suggested to control the speed with torque of sensor-less BLDC motor. The simulation is done on MATLAB/Simulink site and its performance is analyzed with the existing systems, as firefly algorithm (FA) and particle swarm optimization (PSO). Table 1 portrays the implementation of solution techniques.

Fig. 7 shows result of rotor speed variation without controller. Here, the rotor speed raise from 0 to 13.5 rad/s at the time period of 0 to 0.1 s then at 0.1 to 0.5 rotor speed leftovers constant. Fig. 8 portrays result of rotor speed variation of existing FA method. The rotor speed increases 0 to 13.5 rad/s at 0 to 0.1 s time then at 0.1 to 1 s time, the rotor speed leftovers stable. Fig. 9 portrays result of rotor speed variation of existing PSO method. The rotor speed increases 0 to 13.5 rad/s at 0 to 0.12 s time then at 0.1 to 1 s time, the rotor speed leftovers stable.

Fig. 10 depicts the result of rotor speed difference of proposed method. The rotor speed raises from 0 to 13 rad/s at the time period of 0 to 0.1 s then 0.1 to 1 s rotor speed remains stable. Fig. 11 shows the effect of torque variation of without controller. The actual torque flows from 0 to 14 Nm at 0 s then it leftovers stable till the end. Without controller, the torque flows from 0

Table 1  
Implementation of solution systems.

Parameters	Values
FA	
Randomization parameter	0.5
Attractiveness	0.3
Absorption coefficient	1.0
Population size	20
Maximum number of iterations	100
PSO	
C <sub>1</sub> C <sub>2</sub>	1.49446
Population size	100
Range of particle velocity	[−2, 2]

to 21 Nm at 0 s and 0 to 0.1 s the torque of without controller reduced up to 12 Nm at 0.1 to 0.5 s the torque of without controller remains constant till the end. Fig. 12 shows the effect of torque variation of FA method. The actual torque flows from 0 to 14 Nm at 0 s and then it remainders stable till the end. The torque of existing FA method flows from 0 to 17 Nm at 0 s and then the time interval 0 to 0.1 s, the torque of without controller lessened up to 14 Nm at 0.1 s and torque of FA method remainders stable

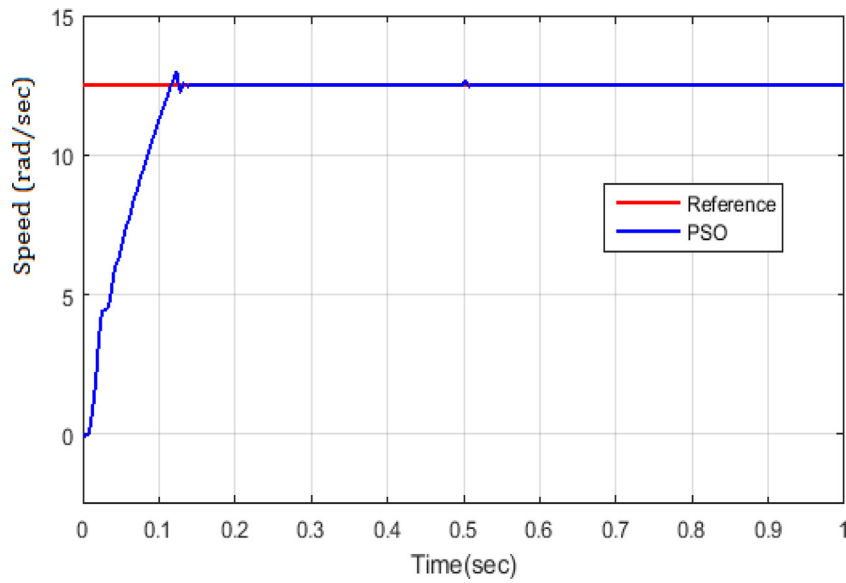


Fig. 9. Result of rotor speed difference of existing PSO method.

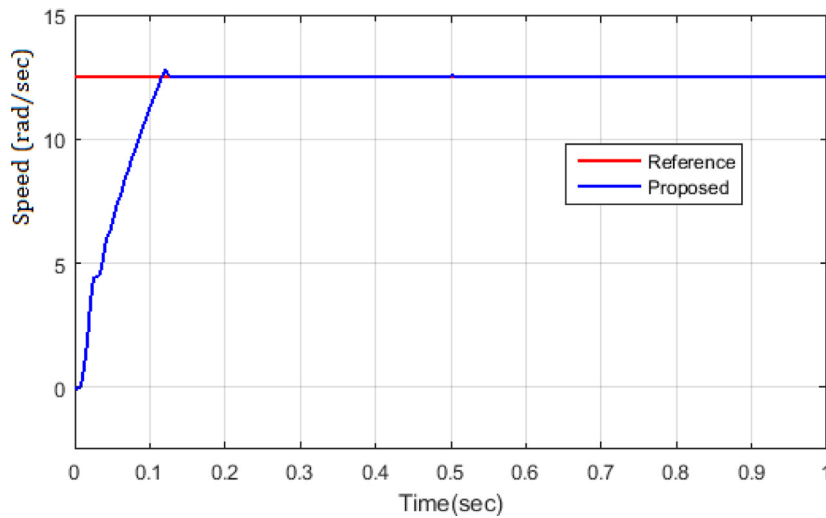


Fig. 10. Result of rotor speed difference of proposed method.

Table 2  
Measurement of Phase voltages.

Degree	Rotor position signal			Switching conditions						Phase voltage (V)		
	A	B	C	sw <sub>1</sub>	sw <sub>2</sub>	sw <sub>3</sub>	sw <sub>4</sub>	sw <sub>5</sub>	sw <sub>6</sub>	V <sub>A</sub>	V <sub>B</sub>	V <sub>C</sub>
0–50	0	0	1	1	0	0	0	0	1	$\frac{v_{DC}}{2}$	0	$-\frac{v_{DC}}{2}$
50–100	0	1	0	0	1	1	0	0	0	$-\frac{v_{DC}}{2}$	$\frac{v_{DC}}{2}$	0
100–150	0	1	1	0	0	1	0	0	1	0	$\frac{v_{DC}}{2}$	$-\frac{v_{DC}}{2}$
150–200	1	0	0	0	0	0	1	0	0	0	$-\frac{v_{DC}}{2}$	$\frac{v_{DC}}{2}$
200–250	1	0	1	1	0	0	1	0	0	$\frac{v_{DC}}{2}$	$-\frac{v_{DC}}{2}$	0

at 0.1 to 0.5 s Fig. 13 shows effect of torque variation with existing PSO method. Here, the actual torque flows from 0 to 14 Nm at 0 s and it remains stable till the end. The torque of existing PSO method flows from 0 to 13 Nm at 0 to 0.1 s and 0.2 s, the torque of PSO method increased up to 14 then the torque of PSO method remains stable at 0.6 to 1 s time.

Fig. 14 portrays effect of torque variation of proposed method. Here, the actual torque flows from 0 to 14 Nm at 0 s and it remains stable till the end. The torque of GEO-RBFNN flows 0 to 16 Nm at 0 s and at 0 to 0.1 s, the torque of proposed method

Table 3  
Performance analysis of torque and speed control using proposed and existing methods.

Solution Technique	Speed in rad/s	Torque in Nm
Without controller	14	10.3
FA	15	11.2
PSO	16	12.35
Proposed method	17	13.43

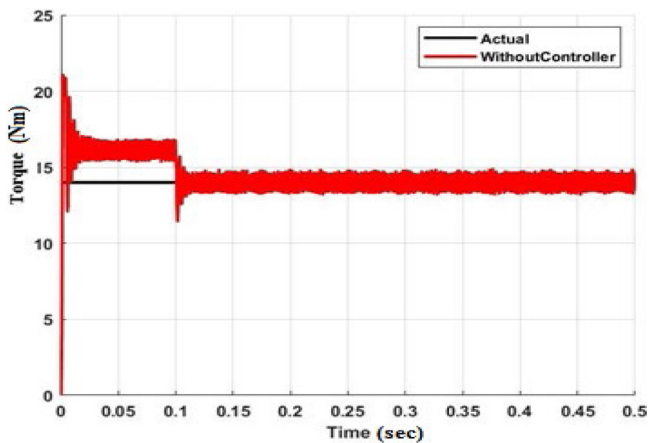


Fig. 11. Impact of torque variation without controller.

Table 4  
Control performance assessment indices of solution techniques.

Solution techniques	Control performance assessment indices			
	ISE	IAE	ITSE	ITAE
FA	0.04129	0.04783	0.0348	0.0359
PSO	0.02162	0.02631	0.08384	0.101
Proposed technique	0.007913	0.00828	0.006182	0.006569

reduced up to 14 Nm then the torque of FA method remains constant at 0.2 to 0.5 s Fig. 15 shows stator current of sensor-less BLDC motor of without controller. Here, current A, current B and current C of without controller are presented. The current A without controller flows 0 to 10 at 0 to 0.05 s and the current A without controller decreased up to 0 and it reduced up to -10 at 0.1 s The current B without controller flows -10 to 0 at 0 to 0.05 s then the current A without controller increased up to 10 and then it suddenly decreased up to -10 at 0.15 s time. The current C without controller flows 0 to -10 at 0 to 0.1 s time and the current A without controller increased up to 0 and it suddenly maximized up to 10 at 0.1 s time. Fig. 16 depicts the stator current of sensor-less BLDC motor of existing FA method with PID controller. Here, current A, current B and current C of without controller are presented. The current A of existing FA method flows from 0 to 10 at the 0 s then the current A of FA method reduced up to -10. The current B of existing FA method flows from 0 to 10 at 0 to 0.1 s and then the current B of FA method reduced up to -10. The current C of FA method flows 0 to -10 at 0 to 0.1 s and the current C of FA method increased up to 10. Fig. 17 shows the stator current of sensor-less BLDC motor of existing PSO through PID controller. Here, current A, current B and current C without controller are presented. The current A of existing PSO method flows to 10 at 0 to 0.1 s then the current A of PSO method reduced up to -10. The current B of existing PSO method flows from -10 to 0 at 0 to 0.01 s and current B of PSO increased up to 10. The current C of existing PSO method flows 0 to -10 at 0 to 0.1 s and the current C of PSO method increased up to 0 and it suddenly raised up to 10 at 0.1 s Fig. 18 depicts stator current of sensor-less BLDC motor of proposed method using PID controller. Here, current A, current B and current C of proposed method are presented. The current A of existing FA flows 0 to 10 at 0 sec then the current A of FA method reduced up to -10. The current B of proposed method d flows from 0 to 10 at 0 to 0.1 s and current B of GEO-RBFNN reduced up to -10. The current C of proposed method flows 0 to -10 at 0 to 0.1 s and the current C of FA maximized up to 10. Fig. 19 shows the stator EMF of sensor-less BLDC motor with proposed method based PID

controller. Here, EMF A, EMF B and EMF C of proposed method are presented. The EMF A of GEO-RBFNN flows 0 to 10 at 0 s and EMF A of GEO-RBFNN reduced up to -10. The EMF B of proposed method flows from 0 to 10 at the time period of 0 to 0.1 s and then the EMF B of proposed method reduced up to -10. The EMF C of proposed method flows 0 to -10 at 0 to 0.1 s and the EMF C of GEO-RBFNN maximized up to 10. Fig. 20 portrays comparative analysis of speed variation of GEO-RBFNN and existing methods. Here, the GEO-RBFNN flows 0 to 16 rad/s at 0 s and it reduced up to 14 rad/s at 0.1 s, then the proposed method remains steady at 0.1 to 0.5 s and rotor speed of GEO-RBFNN reduced up to 12 rad/s at 0.5 and it remains stable until end. The existing FA method flows from 0 to 17 rad/s at 0 s and it reduced up to 16 rad/s at 0.1 s, then the GEO-RBFNN method remains steady at 0.1 to 0.5 s and the rotor speed of GEO-RBFNN reduced up to 12 rad/s at 0.5 and it remains stable until the end. The existing PSO method flows 0 to 16 rad/s at 0 s and it reduced up to 14 rad/s at 0.1 s then the GEO-RBFNN method remains steady at 0.1 to 0.5 s and the rotor speed of GEO-RBFNN method reduced up to 12 rad/s at 0.5 then it remainders steady until the end. The without controller flows 0 to 21 rad/s at 0 s and it reduced up to 16 rad/s at 0.1 s then the GEO-RBFNN method remains steady at 0.1 to 0.5 s and the rotor speed of GEO-RBFNN method reduced up to 12 rad/s at 0.5 then it remainders steady until the end. Fig. 21 portrays comparative analysis of torque variation of proposed and existing systems. Here, the torque of proposed system flows 12 to 23 Nm at 0.02 s time then it decreased up to 14 Nm at 0.04 s and the GEO-RBFNN also reduced up to 12 Nm at 0.14 s then it remains steady at 0.14 to 0.5 s then the torque of GEO-RBFNN lessened up to 11 Nm at 0.5 and then it leftovers stable till the end. The torque of existing FA flows 0 to 15 Nm at 0 to 0.12 s then it reduced up to 12 Nm at 0.12 s time then the torque of FA method remains constant at 0.1 to 0.5 s then the torque of FA method reduced up to 11 Nm at 0.5 and then it remains stable till the end. The torque of existing PSO method flows from 12 to 26 Nm at 0 s and it lessened up to 12 Nm at 0.04 s time also the torque of PSO method reduced up to 5 Nm at 0.12 s and then it leftovers stable till the time of 0.5 s The torque of without controller flows from 12 to 21 Nm at 0 s and it reduced up to 14 rad/s at 0.02 s then it maintains stable at 0.2 to 0.5 s The torque of without controller reduced up to 7 Nm at 0.5 and then it remains stable till the end. Fig. 22 shows performance analysis of proposed torque and speed control with existing methods. The speed of BLDC motor is 14 rad/s, torque is 10.3 Nm using without controller, speed is 15 rad/s, torque is 11.2 Nm for FA method, speed is 16 rad/s, torque is 1.35 Nm for PSO method, and speed is 17 rad/s, torque is 13.43 Nm for proposed method. Here, the proposed system offers better performance than existing systems.

Table 2 shows the measurement of phase voltages. The measurement of phase voltage depends on the rotor position signal and switching conditions. Table 3 portrays performance analysis of proposed torque and speed control with existing methods. The speed of BLDC motor is 14 rad/s, torque is 10.3 Nm using without controller, speed is 15 rad/s, torque is 11.2 Nm for FA method, speed is 16 rad/s, torque is 1.35 Nm for PSO method, and speed is 17 rad/s, torque is 13.43 Nm for proposed method. Control performance assessment indices of solution techniques are displayed in Table 4. Steady-state performance of solution techniques is tabulated in Table 5.

Table 6 tabulates model fitted at entire accessible sample along the results of process for 5 cut-off points:

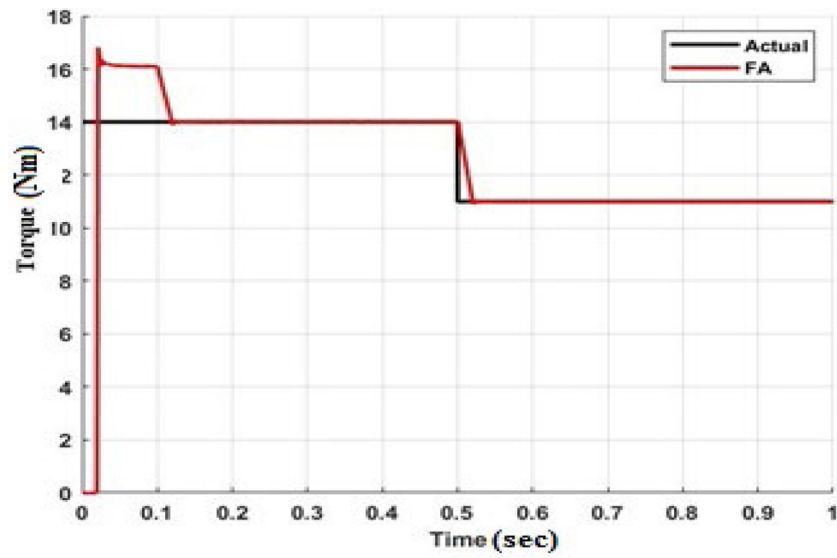


Fig. 12. Impact of torque variation of existing FA method.

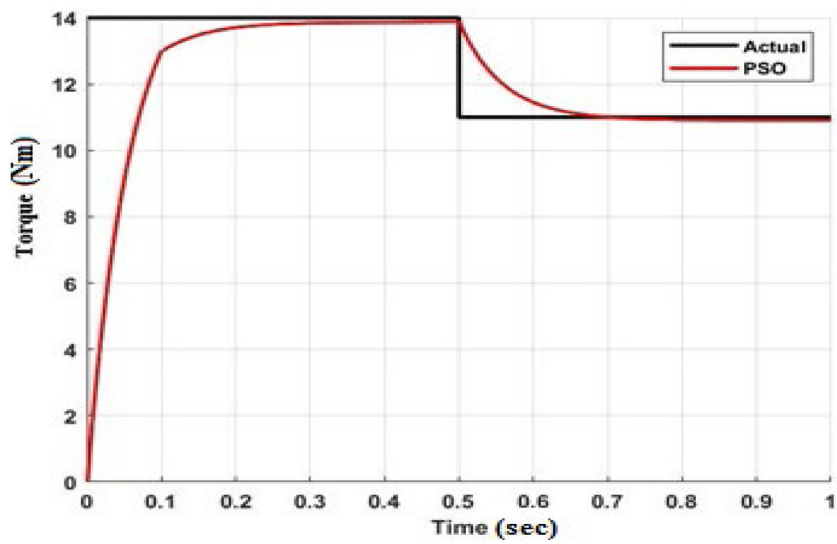


Fig. 13. Impact of torque variation of existing PSO method.

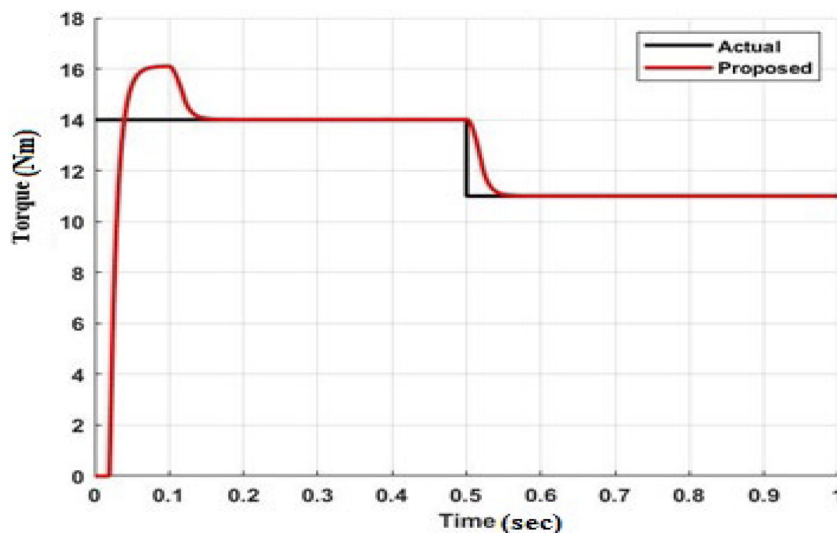


Fig. 14. Impact of torque variation of proposed method.

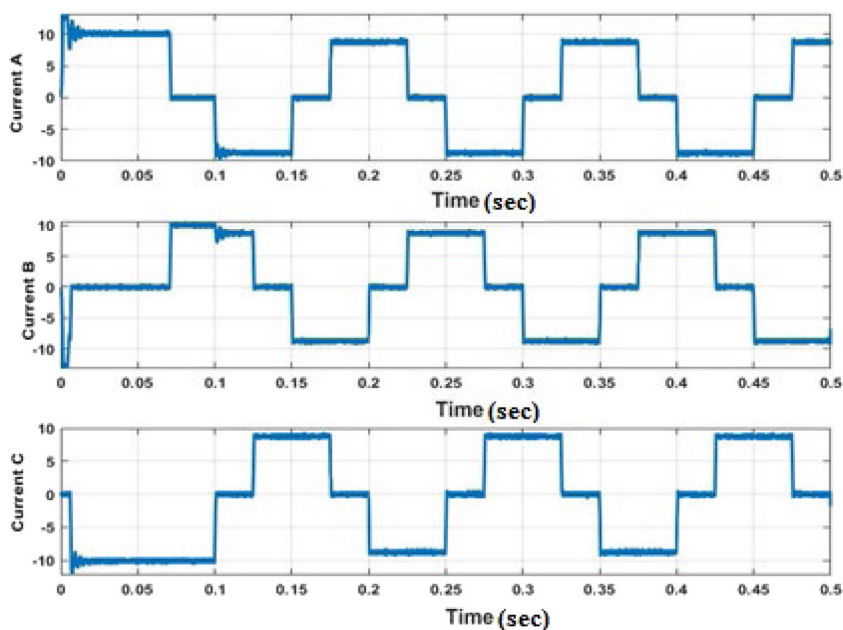


Fig. 15. Stator current of sensor-less BLDC motor of without controller.

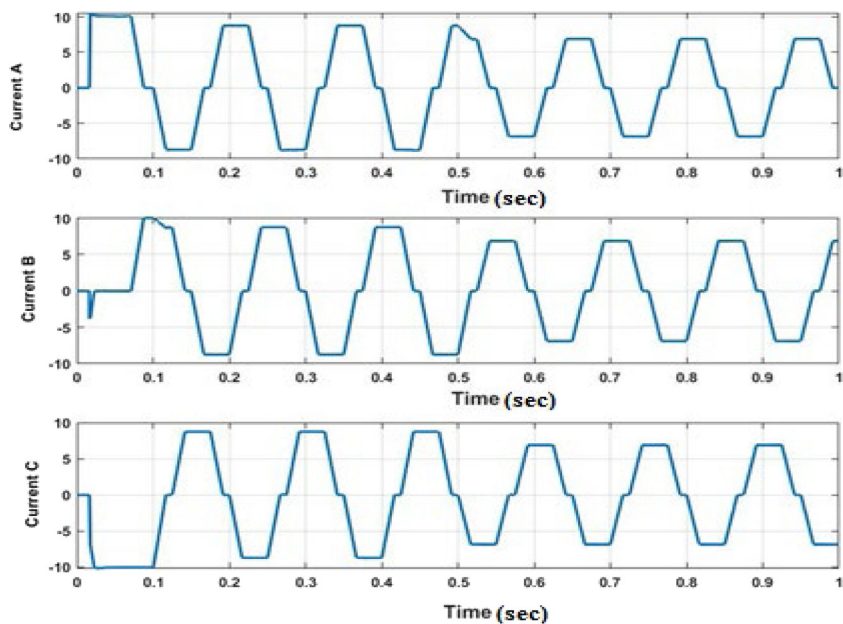


Fig. 16. Stator current of sensor-less BLDC motor of existing FA method.

**Table 5**  
Steady-state performance of solution techniques.

Solution techniques	% THD in stator current	Power factor	Torque ripple	Execution time	Cost benefit analysis
FA	3.13	0.9951	7.4	6.8	Moderate
PSO	6.79	0.9950	13.5	14.5	High
Proposed technique	1.26	0.9978	6.1	5.51	Optimal value

The model fitted with overall accessible data on 1st column, fitting model with 80% accessible data on 2nd column, 75% accessible data in 3rd column, 70% accessible data in 4th column, 66% accessible data in 5th column, 50% in 6th column.

Here, the enormous part of the accessible data reserved to validation samples, the small variance of model estimates, the worse calibration of model at the validation samples. Efficiency comparison of power portrays at Table 7. The copper, Brushless

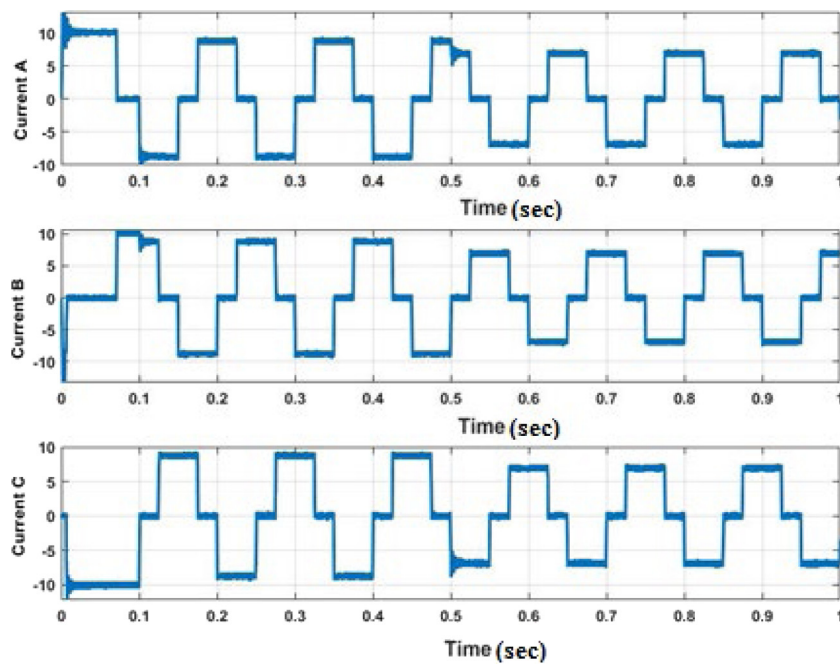


Fig. 17. Stator current of sensor-less BLDC motor of existing PSO method.

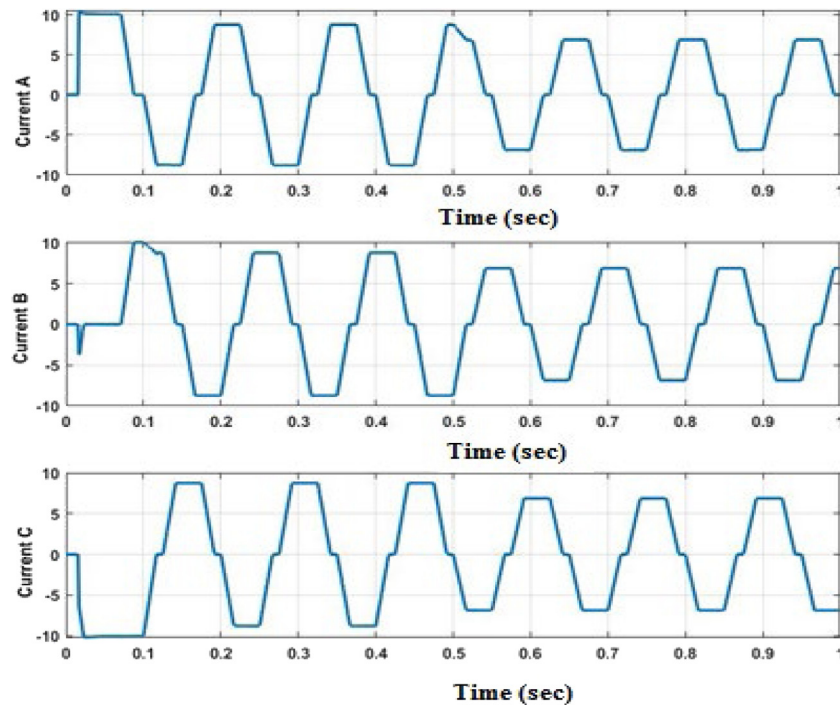


Fig. 18. Stator current of sensor-less BLDC motor of proposed method.

**Table 6**  
Optimal size determination for fitting and validation samples.

Data splitting: optimum cut-off point – 100 iterations

Solution strategy fitting size	100%		80%		75%		70%		66%		50%	
	All sample	Median	-CVar									
FA	5.64	5.7	32	5.3	38	5.6	48	5.6	56	6.3	87	
PSO	0.22	0.2	69	0.715	25	0.2	115	0.2	101	0.3	134	
GEO-RBFNN	0.42	0.481	27	0.733	23	0.520	39	0.517	36	0.53	39	

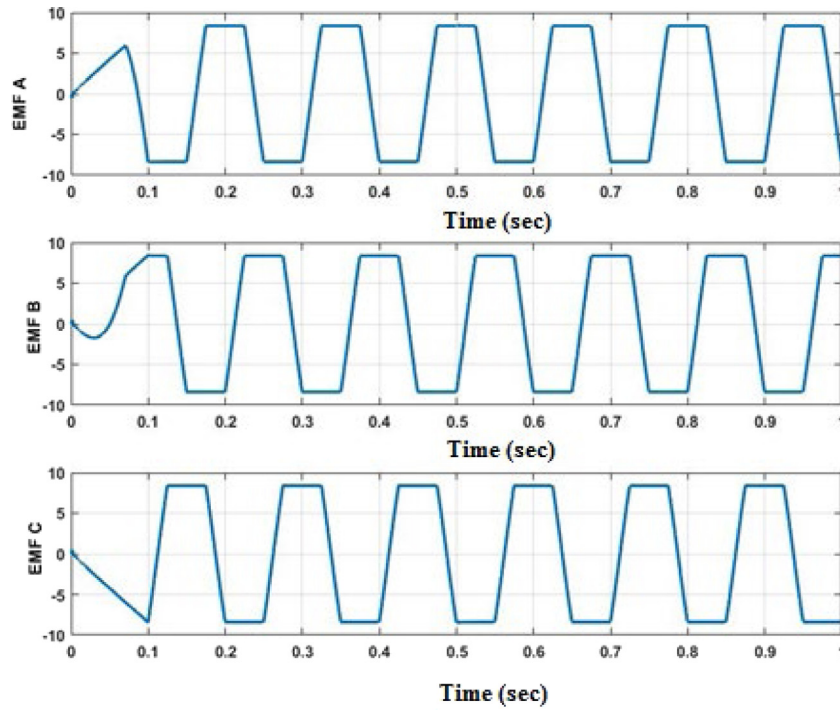


Fig. 19. Stator EMF of sensor-less BLDC motor using GEO-RBFNN based PID controller.

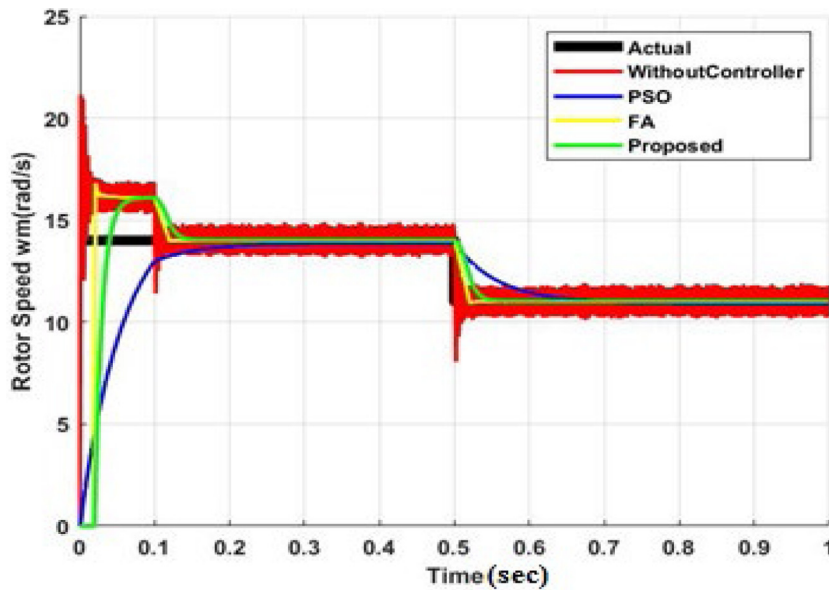


Fig. 20. Comparative analysis of speed variation of GEO-RBFNN and existing methods.

**Table 7**  
Comparison of proposed and existing systems.

Solution	Efficiency (%)
FA	82.137
PSO	77.26589
Proposed	97.99039

### 6. Conclusion

In this manuscript, a novel technique has been performed for controlling speed and torque ripple minimization of BLDC motor. The GEO-RBFNN model is done on MATLAB/Simulink platform; its performance is compared to existing FA and PSO methods. The proposed system provides better result than the existing methods. Among the 5 cut off points, the best one (proposed approach) is 75%. The efficiency of FA, PSO and proposed method is 82.136%, 77.26588% and 97.99038%. The efficiency of proposed

DC core, effectiveness in (%), friction and windage losses in (W) are shown in Table 8.

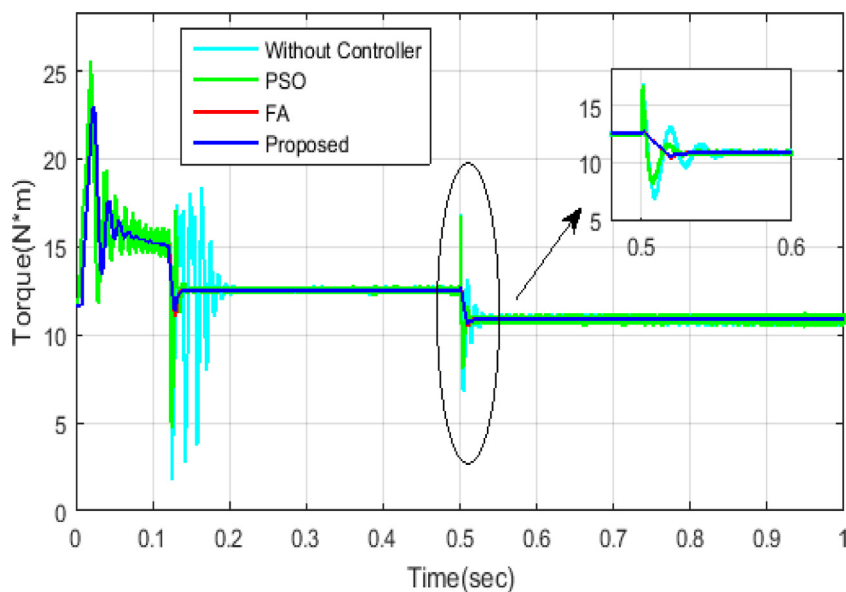


Fig. 21. Comparative analysis of torque variation for GEO-RBFNN and existing methods.

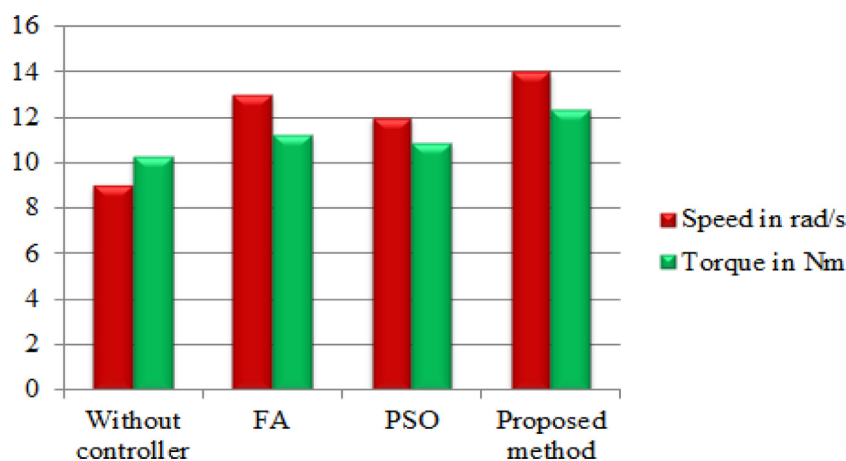


Fig. 22. Performance of torque with speed control of GEO-RBFNN and existing systems.

**Table 8**  
Copper, Brushless DC core, effectiveness in (%), friction and windage losses on (W).

Topology	Copper losses	Core losses	Friction and windage losses	Cumulative losses	Overall effectiveness of drive
[36]	1701.15	219.40	120	2040.55	90.74
[36]	2318.93	180.82	120	2619.75	88.42
[36]	1724.73	251.32	120	2096.05	90.51
[36]	1486.33	269.96	120	1876.29	91.42
Proposed technique	1325.67	270.99	121	1871.17	92.05

method has raises the computational efficiency. To high-power systems with high rotational speed, the control model has limited control performance. The GEO-RBFNN method provides a reliable outcome with lesser count of iterations. The GEO-RBFNN supports to do the calculations simple and provides less difficulty. In future work, we will consider adopting appropriate algorithms to realize the adaptive tuning of controller parameters for assuring the system stability under complex working stages. Moreover, the stability of proposed method will be discussed in the frequency domain.

**Declaration of competing interest**

The authors declare that they have no known competing financial interests or personal relationships that could have appeared to influence the work reported in this paper.

**Data availability statement**

Data sharing does not put on to this article as no novel data has been formed or investigated under this study.

## Funding information

This research did not obtain any exact grant as funding agencies on public, commercial, or not-for-profit sectors.

## References

- [1] Chen X, Liu G. Sensorless optimal commutation steady speed control method for a nonideal back-EMF BLDC motor drive system including buck converter. *IEEE Trans Ind Electron* 2019;67(7):6147–57.
- [2] Li Z, Wang J, Zhou L, Liu X, Jiang F. Enhanced generalized vector control strategy for torque ripple mitigation of IPM-type brushless DC motors. *IEEE Trans Power Electron* 2019;34(12):12038–49.
- [3] Varshney A, Gupta D, Dwivedi B. Speed response of brushless DC motor using fuzzy PID controller under varying load condition. *J Electr Syst Inf Technol* 2017;4(2):310–21.
- [4] Chen S, Liu G, Zhu L. Sensorless control strategy of a 315 kW high-speed BLDC motor based on a speed-independent flux linkage function. *IEEE Trans Ind Electron* 2017;64(11):8607–17.
- [5] Zhang H, Liu G, Zheng S, Zhou X. High-precision sensorless optimal commutation deviation correction strategy of BLDC motor with asymmetric back-EMF. *IEEE Trans Ind Inf* 2020.
- [6] Cui C, Liu G, Wang K, Song X. Sensorless drive for high-speed brushless DC motor based on the virtual neutral voltage. *IEEE Trans Power Electron* 2014;30(6):3275–85.
- [7] Liu G, Chen S, Zheng S, Song X. Sensorless low-current start-up strategy of 100-kW BLDC motor with small inductance. *IEEE Trans Ind Inf* 2016;13(3):1131–40.
- [8] Lee AC, Fan CJ, Chen GH. Current integral method for fine commutation tuning of sensorless brushless DC motor. *IEEE Trans Power Electron* 2017;32(12):9249–66.
- [9] Yang L, Zhu ZQ, Bin H, Zhang Z, Gong L. Safety operation area of zero-crossing detection-based sensorless high-speed BLDC motor drives. *IEEE Trans Ind Appl* 2020;56(6):6456–66.
- [10] Gobinath S, Madheswaran M. Deep perceptron neural network with fuzzy PID controller for speed control and stability analysis of BLDC motor. *Soft Comput* 2019;1–20.
- [11] Viswanathan V, Seenithangom J. Commutation torque ripple reduction in the BLDC motor using modified SEPIC and three-level NPC inverter. *IEEE Trans Power Electron* 2017;33(1):535–46.
- [12] Maharajan MP, Xavier SAE. Design of speed control and reduction of torque ripple factor in BLDC motor using spider based controller. *IEEE Trans Power Electron* 2018;34(8):7826–37.
- [13] Lee W, Kim JH, Choi W, Sarlioglu B. Torque ripple minimization control technique of high-speed single-phase brushless DC motor for electric turbocharger. *IEEE Trans Veh Technol* 2018;67(11):10357–65.
- [14] Trivedi MS, Keshri RK. Evaluation of predictive current control techniques for PM BLDC motor in stationary plane. *IEEE Access* 2020;8:46217–28.
- [15] Naseri F, Farjah E, Schartz E, Lu K, Tashakor N. Predictive control of low-cost three-phase four-switch inverter-fed drives for brushless DC motor applications. *IEEE Trans Circuits Syst I Regul Pap* 2020.
- [16] Cheshmehbeigi HM, Karami E. Maximum output torque control in improved flux path homopolar brushless DC motor with auxiliary field by using optimal control of turn-on and turn-off angles in variable speed applications. *IEEE J Emerg Sel Top Power Electron* 2018;6(4):1722–31.
- [17] de Almeida PM, Valle RL, Barbosa PG, Montagner VF, Ćuk V, Ribeiro PF. Robust control of a variable-speed BLDC motor drive. *IEEE J Emerg Sel Top Ind Electron* 2020;2(1):32–41.
- [18] Bae J, Lee DH. Position control of a rail guided mover using a low-cost BLDC motor. *IEEE Trans Ind Appl* 2018;54(3):2392–9.
- [19] Usman A, Rajpurohit BS. Comprehensive analysis of demagnetization faults in BLDC motors using novel hybrid electrical equivalent circuit and numerical based approach. *IEEE Access* 2019;7:147542–147552.
- [20] Zhou X, Chen X, Peng C, Zhou Y. High performance non salient sensorless BLDC motor control strategy from standstill to high speed. *IEEE Trans Ind Inf* 2018;14(10):4365–75.
- [21] Khazaee A, Abootorabi H, Markadeh GA, Mosaddegh H. MTPA strategy for direct torque control of brushless DC motor drive. *IEEE Trans Ind Electron* 2020.
- [22] Ganesan R, Suresh S, Sivaraju SS. ANFIS based multi-sector space vector PWM scheme for sensorless BLDC motor drive. *Microprocess Microsyst* 2020;76:103091.
- [23] Senthilnathan A, Palanivel P. A new approach for commutation torque ripple reduction of FPGA based brushless DC motor with outgoing phase current control. *Microprocess Microsyst* 2020;75:103043.
- [24] Patel H, Chandwani H. Simulation and experimental verification of modified sinusoidal pulse width modulation technique for torque ripple attenuation in brushless DC motor drive. *Eng Sci Technol* 2021;24(3):671–81.
- [25] Zhang H, Li H. Fast commutation error compensation method of sensorless control for MSCMG BLDC motor with non-ideal back EMF. *IEEE Trans Power Electron* 2020.
- [26] Kommula BN, Kota VR. Direct instantaneous torque control of brushless DC motor using firefly algorithm based fractional order PID controller. *J King Saud Univ Eng Sci* 2020;32(2):133–40.
- [27] de Castro AG, Pereira WCA, de Almeida TEP, de Oliveira CMR, de Almeida Monteiro JRB, de Oliveira AA. Improved finite control-set model-based direct power control of BLDC motor with reduced torque ripple. *IEEE Trans Ind Appl* 2018;54(5):4476–84.
- [28] Dasari M, Reddy AS, Kumar MV. Modified Luo converter based FOPID controller for torque ripple minimization in BLDC drive system. *J Ambient Intell Humaniz Comput* 2022;1–18.
- [29] Santra SB, Chatterjee A, Chatterjee D, Padmanaban S, Bhattacharya K. High efficiency operation of brushless DC motor drive using optimized harmonic minimization based switching technique. *IEEE Trans Ind Appl* 2022.
- [30] He Y, Zheng S, Fang J. Start-up current adaptive control for sensorless high-speed brushless DC motors based on inverse system method and internal mode controller. *Chin J Aeronaut* 2017;30(1):358–67.
- [31] Idris NRN, Toh CL, Elbuluk ME. A new torque and flux controller for direct torque control of induction machines. *IEEE Trans Ind Appl* 2006;42(6):1358–66.
- [32] Singh B, Kushwaha R. A PFC based EV battery charger using a bridgeless isolated SEPIC converter. *IEEE Trans Ind Appl* 2019;56(1):477–87.
- [33] Prabhu P, Urundady V. One-cycle controlled bridgeless SEPIC with coupled inductors for PAM control-based BLDC drive. *Arab J Sci Eng* 2019;44(8):6987–7001.
- [34] Mohammadi-Balani A, Nayeri MD, Azar A, Taghizadeh-Yazdi M. Golden eagle optimizer: A nature-inspired metaheuristic algorithm. *Comput Ind Eng* 2021;152:107050.
- [35] Rajasekaran R, Rani PU. Combined HCS-RBFNN for energy management of multiple interconnected microgrids via bidirectional DC-DC converters. *Appl Soft Comput* 2021;99:106901.
- [36] Ananth DVN. Torque ripple reduction of a brushless DC motor using Y-source converter. *J Eng Res* 2021.